2026 IEEE International Conference on Robotics and Automation (ICRA 2026)
June 1-5, 2026. Vienna, Austria

A Spatiotemporal Brain Activity Visualization and Assessment Framework for Human-Robot Cognitive Interaction Training

Zonghai Huang, Lianchi Zhang, Jingting Zhang*, Fengjun Mu, Rui Huang, Hong Cheng

Abstract— **Accurately assessing brain activity to modulate training parameters online is crucial for improving the human-robot cognitive interaction (HRCI) performance in closed-loop brain training. The major challenge for this technique lies in how to accurately model and characterize the intrinsic behavior of brain activity in HRCI process, which typically exhibits a dynamic manner across spatial and temporal scales. In this study, we propose a dynamic perspective to visualize the spatiotemporal evolution of brain activity during HRCI process, thus enabling assessment of brain states and adaptive modulation during rehabilitation. A novel framework is developed to model the spatiotemporal dynamics of brain activity by integrating deterministic learning with neural population theory. It demonstrates a remarkable capability to mine and visualize the complex nonlinear dynamics of brain activity, encompassing both temporal evolution and spatial connectivity patterns. The proposed model not only visualizes of spatiotemporal brain dynamics but also enables online assessment of brain states, which can facilitate optimal modulation of HRCI process and improve the brain training efficiency. The method is validated using a panoramic virtual reality system. Results show that our method improves the accuracy of brain activity assessment by 8.86%, effectively demonstrating that it accurately visualizes spatiotemporal brain dynamics and enhances training outcomes when integrated with HRCI.**

I. INTRODUCTION

Human-Robot Cognitive Interaction (HRCI) technology is crucial for closed-loop brain training paradigm, in which brain or physiological signals are continuously monitored to guide adaptive robot behavior [1]. The robot delivers multimodal sensory feedback via visual, auditory, or haptic channels, thereby establishing dynamic and bidirectional interaction. This paradigm incorporates user states into the control loop and transforms training from one-way stimulation into adaptive human–robot collaboration [2]. A representative rehabilitation application of HRCI is Neurofeedback Training (NFT), where robots provide targeted feedback based on neural measurements, including electroencephalography (EEG) or functional Near-Infrared Spectroscopy (fNIRS) [3]. This process actively engages patients in rehabilitation, thereby making the training both interactive and personalized.

This work was supported in part by the National Natural Science Foundation of China (Grant 62403104, 62473079), the Sichuan Science and Technology Program (Grant 2025ZNSFSC1518), the Fundamental Research Funds for the Central Universities (Grant ZYGX2024XJ028), the Foundation of Nursing Key Laboratory of Sichuan Province (Grant No. HLKF2024(Z)-3).

Zonghai Huang, Lianchi Zhang, Jingting Zhang and Fengjun Mu are with School of Automation Engineering, University of Electronic Science and Technology of China, 611731, China. Hong Cheng is with School of Mechanical and Electrical Engineering, University of Electronic Science and Technology of China, 611731, China. ⋆Corresponding author: Jingting Zhang, zhangjt@uestc.edu.cn

In NFT, multimodal stimulation engages multiple brain regions simultaneously, promoting coordinated activation, which increases the likelihood of neuronal synchronization and strengthens inter-regional connectivity. This multidimensional paradigm supports neuroplasticity more effectively, leading to comprehensive and efficient recovery. It also enables rehabilitation to be tailored to individual needs [4]. Achieving these benefits requires continuous monitoring of the functional states of different brain regions [5]. Capturing the spatiotemporal dynamics of brain activity allows NFT to quantify training effects precisely and provides a basis for refining rehabilitation strategies. Obviously, visualizing spatiotemporal dynamics is crucial for assessing brain activity and enabling adaptive modulation of rehabilitation training.

Accurate visualization of brain spatiotemporal dynamics is essential for assessing neural activity and guiding NFT. Spatial approaches, such as Dynamic Causal Modeling (DCM) [6], Granger causality [7], and graph-based methods including Graph Convolutional Neural Networks (GCNN) [8], primarily investigate structural or functional dependencies between brain regions. Their goal is to map connectivity patterns underlying neural processes. Temporal approaches, including statistical correlation analysis and sequential models such as Long Short-Term Memory (LSTM) [9] and Convolutional Neural Networks (CNN) [10], emphasize the dynamic evolution of neural signals over time, enabling the detection of state transitions and temporal regularities. Integrated spatiotemporal approaches combine these perspectives to jointly capture distributed spatial interactions and their temporal variations, providing a more holistic representation of brain activity. However, despite these advances, existing approaches often struggle to capture the complex intrinsic nonlinear dynamics of neural systems, which limits the interpretability of derived representations and their ability to reliably track evolving cognitive states for adaptive NFT.

Recently, Deterministic Learning (DL) has been applied to model the nonlinear dynamics of biological systems, including cardiovascular signals [11], respiration [12], and gait [13]. DL offers a computational and interpretable framework to capture intrinsic patterns and store dynamic knowledge in constant radial basis function neural networks (RBF NNs). Therefore, extending DL to neural signals enables interpretable characterization of regional activation and spatiotemporal brain dynamics. With its high temporal resolution, EEG is particularly suitable for such modeling compared to fMRI and fNIRS. However, existing DL-based schemes have not fully addressed the challenge of modeling brain activity across multiple spatial and temporal scales

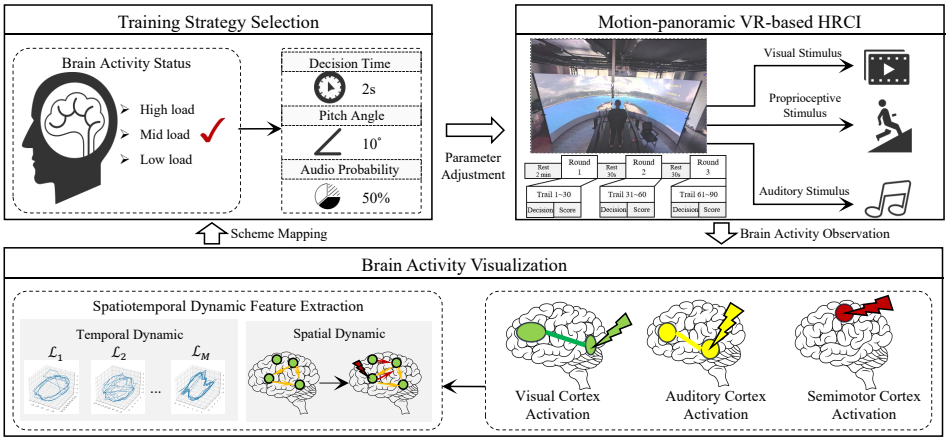

Fig. 1. Overview of the proposed human-robot cognitive interaction training paradigm based on panoramic VR platform.

under intrinsic cognitive processes and extrinsic stimulation, thereby limiting their application in neural dynamics modeling, spatiotemporal visualization, and status assessment.

In this work, we present a spatiotemporal dynamical visualization framework for HRCI that enables accurate representation of brain activity and enhances the effectiveness of personalized training. EEG signals are analyzed using DL to extract spatiotemporal dynamic features of brain activity, enabling visualization of evolving brain states. Brain activity derived from these features provides a key metric for adaptive task modulation in the NFT paradigm. Experimental results demonstrate that, compared with pre-training assessments using standardized cognitive scales, the proposed paradigm more effectively enhances participants' training outcomes. Furthermore, the spatiotemporal feature–based classification method improves accuracy by 8.86% relative to existing models.

The contributions of this study are as follows.

i) An innovative panoramic virtual reality (VR)-based HRCI paradigm that integrates immersive multimodal feedback across visual, auditory, and haptic channels to maximize engagement and induce adaptive cognitive responses during interaction.

ii) A DL-based framework for extracting and visualizing spatiotemporal brain dynamics, providing interpretable characterization and accurate assessment of evolving brain activity states.

iii) Comprehensive experimental validation demonstrating improved accuracy in brain activity classification and significant enhancement of participants' cognitive control using the proposed paradigm.

II. Panoramic VR-based Human–Robot Cognitive Interaction Paradigm for Brain Training

As shown in Fig. 1, the proposed HRCI paradigm is implemented on the panoramic VR platform, which combines 3D visual presentations, multi-channel auditory feedback, and central motion perturbations to deliver immersive cognitive experiences. Within this framework, spatiotemporal features of brain dynamics extracted from EEG signals are used to identify distinct brain states, which in turn guide adaptive adjustment of task difficulty. Task parameters such as decision time, the probability of auditory stimulus events, and the pitch angle of the platform are dynamically modulated to match cognitive states of participants.

The protocol integrates two classical cognitive decision-making paradigms, the Ultimatum Game and the Iowa Gambling Task, into a rowing competition implemented on the panoramic VR system to provide quantifiable measures of decision outcomes. In each trial, participants decide whether to accept one of three score allocation strategies presented randomly (3 vs. 7, 5 vs. 5, or 7 vs. 3), with a 50% chance of outcome correction for unfair allocations. Decisions are executed through center-of-gravity shifts, and task performance is continuously conveyed through immersive multimodal feedback. This includes maritime scenes projected on a 180° curved screen, spatialized environmental sounds with valence-specific cues, and real-time motion perturbations through a three-degree-of-freedom platform. Visual feedback displays both players' scores and rowing distances, while auditory and motion cues reinforce decision outcomes and enhance ecological validity.

TABLE I
Paradigm Parameters Under Different Brain Activities

Brain Activity	Time (s)	Aud. Prob. (%)	Pitch Angle (°)
Low	1	75	20
Mid	2	50	10
High	3	25	0

Each participant completed two experimental sessions. In the first session, decision and feedback timing were fixed, following the immersive protocol in [14]. In the second session, real-time EEG signals were analyzed to recognize brain activity states, which guided adaptive modulation of task parameters. Specifically, decision time (1, 2, 3s), probability of auditory stimulus events (25%, 50%, 75%), and platform pitch angle (0°, 10°, 20°) were dynamically modulated, as summarized in Table I. This adaptive mechanism ensured that task difficulty was continuously adapted to each participant's evolving cognitive and motor states.

Within this paradigm, closed-loop human–robot interaction is achieved through bidirectional information flow. Participants' EEG signals and decision-making are used to continuously assess cognitive load and adapt task parameters in real time. In turn, the robot delivers immersive multimodal

feedback through visual, auditory, and motion cues, which shape participants' strategies and support cognitive regulation. By linking ongoing brain-state assessment with adaptive feedback, the system establishes an integrated HRCI loop that enhances engagement, promotes cognitive flexibility, and strengthens motor coordination throughout the task.

III. Brain Dynamics Modeling for Visualization and Assessment

Personalized modulation of immersion during HRCI requires continuous assessment of participants' brain activity to enhance engagement throughout the training. EEG provides an effective neural measure for online characterization of brain dynamics. Based on this, we propose an EEG-based framework for brain activity visualization (Fig. 2). Brain activity is modeled as a dynamical system, and DL is employed to extract its underlying dynamics. The spatiotemporal properties of brain activity are then quantified using the maximum Lyapunov exponent (LYE) and Pearson correlation. These metrics serve as input features to a classifier for real-time evaluation of brain states.

A. Mathmatical Description for Spatiotemporal Brain Activity

Brain activity exhibits nonlinear dynamics, and commonly used modeling approaches include DCM. Typically, brain activity modeling involves two components: i) modeling the latent neural states (neurodynamics) that describe the evolution of brain activity over time, and ii) modeling the observation process (neural populations) that links these hidden states to measurable signals. The corresponding mathematical formulations are provided below:

$$\dot{X} = f(X, U, \theta) \tag{1}$$

$$h_j = g_j(x_j, \theta) \tag{2}$$

The first equation describes the spatiotemporal neurodynamics, where $X = [x_1, x_2, ..., x_M]$ denotes the hidden neural states, with M representing the total number of observed brain regions. $U = [u_1, u_2, ..., u_N]$ represents external inputs or stimuli, which directly target N brain regions. θ denotes the set of model parameters. The second equation specifies the observation mapping based on neural population theory, in which the hidden states X are transformed into measurable EEG signals $H = [h_1, h_2, ..., h_M]$. The remainder of this section elaborates the state and observation models and integrates them within a unified dynamical framework.

1) Spatiotemporal neurodynamic modeling for brain activation. In neurodynamic modeling, the activity of brain regions is treated as a coherent dynamical process, where each region functions as a computational node whose state is influenced by both intrinsic connectivity and external stimuli. This formulation enables analysis of how local activations propagate through the network, dynamically altering functional relationships. Neurodynamics are commonly described using bilinear differential equations. In the resting state, activation levels and functional connectivity among brain regions are maintained in dynamic equilibrium. This equilibrium can be mathematically represented as $\dot{X} = AX$, providing a basis for modeling the temporal evolution of neural dynamics, where A denotes intrinsic connectivity among functional brain regions at rest. Upon external stimulation, targeted regions undergo direct modulation, while connected regions are influenced through network interactions, producing enhancement or attenuation effects that alter effective connectivity. Consequently, the stimulus-driven brain system can be described by the following bilinear equation:

$$\dot{X} = (A + \sum_{i=1}^{N} B^i u_i)X + CU \tag{3}$$

Here, B denotes the modulation matrix, characterizing changes in inter-regional connectivity following brain activation, while C represents the exogenous input matrix, specifying how external stimuli directly drive the activity of corresponding regions.

2) Neural Population Modeling for EEG Observation. Neuronal population theory provides a conceptual framework for describing the collective dynamics of interacting neurons, representing the activity of large neural ensembles as aggregate state variables rather than tracking individual spikes. This abstraction enables characterization of macroscopic neural dynamics underlying EEG signals. Based on this principle, DCM extends neuronal population theory to infer effective connectivity among brain regions from EEG observations. In DCM, each brain region is modeled as a neural mass whose state evolves according to intrinsic connections and context-dependent modulatory influences. This neuronal population model captures how local neural activity propagates through the network to generate observed EEG signals, establishing a mechanistic link between regional neural dynamics and measurable electrophysiological responses. Following this framework, the observed EEG signals can be expressed as a function of the underlying neural states. Let x_j denote the state of the neuronal population in the j_{th} region, then the measured signal h_j is given by $h_j = g_j(x_j, \theta)$. In classical DCM, this mapping is often approximated as a linear transformation of the neuronal states:

$$h_j = Lx_j \tag{4}$$

Here, L is a lead-field matrix, accounting for the passive conduction of the electromagnetic field. By combining Eqs. (4) and (5), the brain activation system can be expressed as a first-order dynamical system in terms of the observed EEG signal. This formulation enables the extraction of latent dynamical information underlying brain activity, providing a principled basis for analyzing the evolution of brain states.

$$\dot{H} = (A + \sum_{i=1}^{N} B^i u_i)L^{-1}H + CU \tag{5}$$

However, the relationship between latent neural states and observed EEG signals is highly complex, involving numerous prior parameters and intricate inter-regional dependencies.

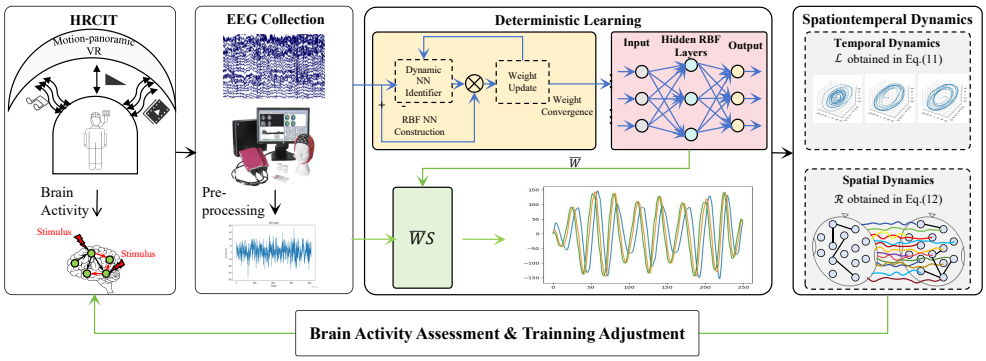

Fig. 2. Overview of the proposed brain activity visualization method using deterministic learning.

This complexity renders direct characterization of the underlying dynamics challenging and limits the effectiveness of conventional analysis. To overcome these limitations, we employ a dynamical modeling approach based on DL, which enables systematic extraction of the latent spatiotemporal features of brain activity.

B. Data Driven Modeling for Brain Dynamics via Deterministic Learning

Given the highly complex relationship between latent neural states and observed EEG signals, which involves numerous prior parameters and intricate inter-regional dependencies, direct characterization of brain dynamics remains challenging. To address this, we employ DL combined with a High-Gain Observer (HGO) to probe latent neural dynamics. The HGO reconstructs unobserved neural states and estimates their temporal derivatives, while DL identifies region-specific dynamic patterns from the measured signals. In the following, we provide a detailed description of the dynamical modeling approach.

1) High-gain observer for latent dynamics extraction. By deriving a low-dimensional representation from single-channel EEG measurements, the HGO enables reconstruction of enables reconstruction of temporally resolved neural dynamics otherwise obscured by the nonlinear complexity of brain activity. Extracting meaningful dynamic features from one-dimensional EEG signals is challenging, as the underlying neural processes are high-dimensional and highly coupled. Following the principle established by Robinson et al. [15], namely that any dissipative system can be approximated by a set of three-dimensional ordinary differential equations, we employ the HGO to recover latent three-dimensional system dynamics from one-dimensional EEG recordings. The HGO is formally defined as follows:

$$r(k+1) = A_d r(k) + B_d h_j(k) \tag{6}$$

$$\hat{v}(k) = C_d r(k) + D_d h_j(k) \tag{7}$$

$\hat{v}(k) = [\hat{v}_1(k), \hat{v}_2(k), \hat{v}_3(k)]$ is the estimated EEG $h_j(k)$, $r(k)$ is the state vector of the observer. The matrix of observer are obtained by the bilinear transformation with $A_d = (I + \frac{\alpha}{2}A_0)(I - \frac{\alpha}{2}A_0)^{-1}$, $B_d = \alpha(I - \frac{\alpha}{2}A_0)^{-1}L_0$, $C_d = D_0^{-1}(I - \frac{\alpha}{2}A_0)^{-1}$, $D_d = \frac{\alpha}{2}C_d L_0$. Where $\alpha = T_s/\epsilon$, A_0 is the third-order displacement matrix, $B_0 = [0,0,1]^T$, $C_0 = [0,0,1]$, $D_0 = diag[1,\epsilon,\epsilon^2]$, $L_0 = [l_1, l_2, l_3]^T$. ϵ is the gain of the observer, L_0 is the roots of Hurwits polynomials, T_s is the sampling period. The brain activition system can be rewritten as $F(\hat{v}(k);\psi)$.

2) Deterministic learning for dynamic patterns. Once the internal state vector $\hat{v}(k)$ is estimated, we can construct the corresponding dynamical identifiers and apply the deterministic learning law to capture and model the underlying respiratory dynamics. The trajectory can be written as:

$$F_i(\hat{v}_i(k);\psi) = \hat{F}_i(\hat{v}_i(k);\psi) + e_i(\hat{v}_i(k)) \tag{8}$$

Where $\hat{F}_i(\hat{v}_i(k);\psi)$ represents the estimate, $e_i(\hat{v}_i(k)$ is modeling uncertainty. The identifier of dynamic system is modeled by a class of RBF NN as follow:

$$\begin{aligned} s_i(k+1) =& s_i(k) + \phi_i(s_i(k) - \hat{v}_i(k)) + \\ & T_s \hat{W}_i^T(k) S_i(\hat{v}_i(k)) \end{aligned} \tag{9}$$

Here, s_i is the state of estimator, ϕ_i is the designed identifier gain in the range $(-1, 0)$, $\hat{W}_i^T(k)S_i(\hat{v}_i(k))$ is the RBF NN with gaussian kernel. The weight of the dynamic system $\hat{W}_i$ is updated according to the following law:

$$\begin{aligned} \dot{\hat{W}}_i(k+1) =& \hat{W}_i(k) - \\ & T_s \beta S_i(\hat{v}_i(k))(s_i(k+1) - \hat{v}_i(k+1)) \end{aligned} \tag{10}$$

β is a hyperparameter according to the sampling interval. Based on deterministic learning theory, the above method ensures that the neural network weights converge rapidly to their optimal values, satisfying the persistent excitation condition of the RBF NN and thus achieving locally accurate approximation of the brain activition system $F_i(\hat{v}_i(k);\psi) \cong \bar{W}_i^T(k)S_i(\hat{v}_i(k))$. $\bar{W}_i = \frac{1}{t_b - t_a + 1}\sum_{k=t_a}^{t_b} \hat{W}_i(k)$ is average weight vector in time $[t_a, t_b]$ after model converge. Finally, the trajectory $\bar{F}_i(\hat{v}_i(k);\psi) = \bar{W}_i^T S_i(\hat{v}_i(k)) = [\bar{F}_{i_1}, \bar{F}_{i_2}, \bar{F}_{i_3}]$ is generated to extract the spatiotemporal dynamic feature of dynamic system using the learned 3D information.

C. Spatiotemporal Dynamics Visualization and Brain Activity Assessment

Spatiotemporal dynamics of brain activity are sensitive to task demands, as both under-challenging and overly demanding tasks can induce dysregulation in temporal variability and large-scale spatial coordination of neural processes. As shown in Fig. 3, we characterize these changes using

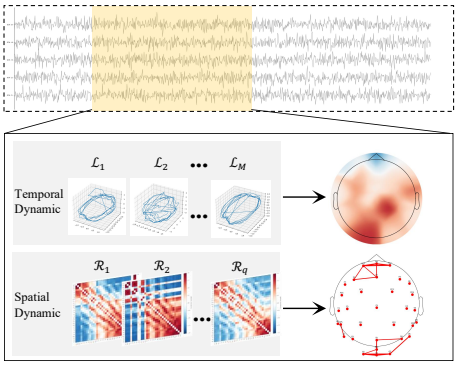

Fig. 3. An overview of spatiotemporal dynamic quanification and brain activity assessment.

two complementary dynamical metrics derived from DL-estimated system dynamics: the LYE and Pearson correlation. These features provide a discriminative representation of brain activity, enabling robust differentiation of mental states and assessment of task-induced neural dynamics.

1) Maximum Lyapunov exponent for temporal dynamics. The LYE is employed to characterize the temporal stability of the dynamical system estimated through DL. Specifically, it quantifies the average exponential rate at which nearby trajectories in the reconstructed state space diverge or converge over time, reflecting the sensitivity of brain dynamics to initial conditions. A large LYE indicates pronounced divergence of trajectories, corresponding to unstable or chaotic neural dynamics, whereas a small LYE indicates stable or weakly varying temporal evolution. The LYE can be calculated as follows:

$$\mathcal{L}_i = \frac{p}{q}\sum_{k=1}^{\frac{q}{p}} ln\left(\frac{\|\bar{F}_i(k_{j_2}) - \bar{F}_i^*(k_{j_2})\|}{\|\bar{F}_i(k_{j_1}) - \bar{F}_i^*(k_{j_1})\|}\right) \tag{11}$$

Where q is the length of $\bar{F}_i$. It first calculate the distance between the initial point $\bar{F}_i(k_{j_1})$ and its nearest point $\bar{F}_i^*(k_{j_1})$. Next, the distance between the two points after p steps at time k_{j_2} is calculated.

2) Pearson correlation for spatial dynamic. The spatial organization of brain activity was modeled as an undirected weighted graph $\mathcal{G} = (\mathcal{N}, \mathcal{E}, \mathcal{R})$, where each node in $\mathcal{N} = \{n_1, n_2, \ldots, n_M\}$ represents a cortical region. The edge set $\mathcal{E}$ encodes potential functional interactions between regions, and the weight matrix $\mathcal{R} = [P_{n_a,n_b}], a \neq b$ specifies the strength of these interactions. This framework provides a compact and mathematically tractable representation of large-scale spatial dynamics, enabling subsequent analysis of inter-regional coordination using network-theoretic metrics such as node degree, clustering coefficient, and global efficiency. To capture the spatial coordination of brain activity, Pearson correlation was calculated between $\bar{F}_{i_1}$ across different channels. This metric reflects the degree of linear synchronization between spatially distributed brain signals, where higher values indicate stronger functional coupling and lower values suggest weakened inter-regional coordination. Formally, the Pearson correlation between n_a and n_b region is calculated as:

$$P_{n_a,n_b} = \frac{Cov(\bar{F}_{i_1,n_a}, \bar{F}_{i_1,n_b})}{\sqrt{Var(\bar{F}_{i_1,n_a})\ Var(\bar{F}_{i_1,n_b})}} \tag{12}$$

$Cov()$ denotes covariance, and $Var()$ is variance. Because the Pearson correlation is inherently symmetric, the resulting connectivity graph forms an undirected network. This framework reflects the degree of synchronization between pairs of brain regions and enables extraction of graph-based metrics, including node centrality, clustering coefficient, average path length, and modular structure. Together, these metrics provide a quantitative characterization of global brain network organization and integration.

3) Brain activity assessment. The assessment of brain activity is formulated as a classification problem based on feature vectors that integrate both temporal dynamics $\mathcal{L} \in R^{N\times 1}$ and spatial interactions $\mathcal{R} \in R^{N\times N}$. Given the high dimensionality of these combined features, the risk of overfitting is substantial. To mitigate this, principal component analysis (PCA) is applied separately to the temporal and spatial domains, yielding compact yet informative representations that preserve the dominant variance in the data. On this reduced feature manifold, a discriminative model is constructed to distinguish brain states, with class boundaries defined to maximize separability in the feature space. This framework enables reliable classification of brain states across multiple levels of brain activity.

IV. Experiment and Results

A. Participants and Experiment Setup

Cognitive load is adopted in this study as a functional index for investigating the spatiotemporal dynamics of brain activity during HRCI. It has been widely recognized as a sensitive indicator of how the brain allocates resources and adapts to varying task demands. Unlike raw neural signals, which primarily capture oscillatory activity, cognitive load reflects higher-order integrative processes that couple neural dynamics with behavioral performance and engagement levels. This makes it particularly suitable for probing how task demands induce temporal variability and large-scale coordination of brain networks. By incorporating cognitive load into the experimental paradigm, we aimed to establish a principled framework for linking brain dynamics to functional states. As illustrated in Fig. 4, participants' neural signals are captured in real time during training, enabling visualization of spatiotemporal trajectories, brain topographies, and connectivity patterns, as well as dynamic adjustment of training parameters. In this study, six healthy subjects were included in the experiment. The EEG data were acquired using a 32-channel setup aligned with the international 10-20 electrode placement system (Waveguard$^{\text{TM}}$Mylab). Each participant completed two experiments: one under maximal immersion and another using a cognitive-load–based adaptive HRCI paradigm, with at least a two-hour interval between them. All participants provided written informed consent before participation, and the study protocol was approved by the

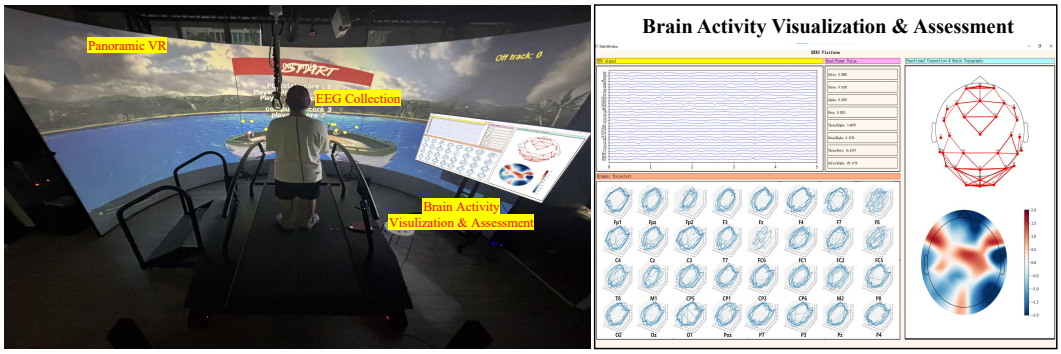

Fig. 4. HRCI training scene with spatiotemporal dynamics–based control.

TABLE II
ELECTRODES EXHIBITING SIGNIFICANT DIFFERENCES IN MAXIMUM LYAPUNOV EXPONENT ACROSS COGNITIVE LOAD CONDITIONS

Electronode	Low Load	Mid Load	High Load	p
T8	2.26±0.68	1.76±0.54	2.16±0.69	**0.00**
CP2	2.32±0.67	2.05±0.61	2.13±0.77	**0.00**
CP6	2.18±0.61	1.97±0.52	2.09±0.76	**0.00**
P7	2.17±0.61	1.67±0.50	2.10±0.80	**0.00**
P3	2.20±0.73	1.83±0.63	2.13±0.63	**0.00**
Pz	2.26±0.72	1.67±0.52	2.11±0.70	**0.00**
P4	2.34±0.69	1.82±0.55	2.17±0.76	**0.00**
P8	2.18±0.69	1.53±0.42	2.09±0.68	**0.00**
POz	2.23±0.74	1.73±0.72	2.22±0.71	**0.00**
O1	2.28±0.69	1.68±0.60	2.21±0.69	**0.00**
Oz	2.26±0.65	1.63±0.44	2.16±0.66	**0.00**
O2	2.17±0.73	1.51±0.51	2.14±0.71	**0.00**

Ethics Committee of University of Electronic Science and Technology of China [No. 34088].

B. Data Preprocessing

To validate the effectiveness of the proposed model in modulating rehabilitation parameters within the HRCI framework, this study evaluated participants' cognitive load based on the extracted spatiotemporal dynamical features, thereby enabling adaptive adjustment of training parameters. The collected 32-channel EEG signals were re-referenced to the whole-brain average and then zero-phase band-pass filtered between 4 and 12 Hz to capture neural oscillations in the θ and α bands, which are highly sensitive to cognitive load variations. The signals were subsequently downsampled to 250 Hz for further analysis.

Participants first completed training under conditions of maximal immersion [14]. EEG data acquired during this session were used to construct a dataset for classifying decision-load levels. The cognitive-load labels were determined based on choice entropy (En), with labeling performed every five trials and categorized into high ($En > \mu + m\delta$), medium ($\mu + m\delta \geq En \geq \mu$), or low ($En < \mu$) levels. Here, μ and δ denote the mean and standard deviation of participants' choice entropy, respectively, and m is a scaling factor, usually set to 0.5. This dataset served for offline training of the decision-load classifier. The resulting model was subsequently employed in a second session to perform online classification of decision-load levels and to adaptively adjust training parameters in real time.

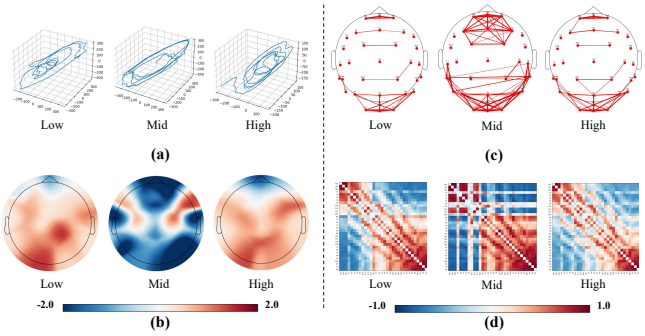

Fig. 5. Spatiotemporal visualization of brain activity: (a) 3D trajectory of Pz electrode. (b) Topographic map based on the maximum Lyapunov exponent. (c) Functional brain network reconstructed from dynamics.

C. Visualization of Spatiotemporal Brain dynamics

The spatiotemporal evolution of brain activity across varying cognitive load levels is summarized in Fig. 5, which integrates complementary perspectives from reconstructed system trajectories, LYE-based topographies, and functional connectivity networks. Together, these visualizations provide converging evidence of how cognitive demands modulate neural dynamics across temporal, regional, and network levels.

The dynamical system trajectories reconstructed via DL (Fig. 5(a)) reveal distinct divergence patterns across load conditions. Under low load, trajectories are loose and dispersed, reflecting insufficient neural activation and limited processing efficiency. At moderate load, trajectories exhibit a structured, hierarchical organization, indicating an optimal balance between stability and complexity that supports efficient information processing. High load produces divergent yet disordered trajectories, suggesting overactivation and instability that impair processing efficiency.

Topographical analysis using LYE (Fig. 5(b)) highlights regional differences in neural stability. Under low load, occipital electrodes (O1, Oz, O2, POz), parietal electrodes (P3, P4, P7, P8, Pz), and additional centro-parietal and temporal sites (T8, CP2, CP6) exhibit elevated LYE values, reflecting instability in visual processing, spatial attention, and temporal–parietal integration when neural resources are limited. Moderate load reduces exponents across the frontal–parietal network and these additional sites, indicating enhanced coordination among executive, working memory,

TABLE III

COGNITIVE LOAD ASSESSMENT RESULTS ACROSS DIFFERENT MODELS

Methods	Acc	Pre	Rec	F1	Kappa
SVM	58.44	67.69	52.29	50.73	0.31
CNN	66.00	65.55	65.60	65.50	0.48
LSTM	58.67	58.95	58.11	57.97	0.37
GCNN	55.11	54.49	54.52	54.21	0.31
EEGNet	67.78	68.94	67.18	67.87	0.50
DeepConvNet	64.00	63.40	64.19	62.05	0.46
EEGTransforemr	68.00	67.19	68.12	67.28	0.51
TCN	68.22	68.31	68.56	67.77	0.52
S-T Transforemr	58.00	56.67	57.18	56.72	0.35
Ours	**77.08**	**77.10**	**76.51**	**76.54**	**0.65**

and multimodal integration regions. High load again elevates exponents in occipital, parietal, and temporal–centroparietal areas, suggesting overburdened visual pathways and a mismatch between sensory input and higher-order cognition. These observations are quantitatively confirmed by LYE scores across the same electrodes (Table II), showing elevated LYE under low and high loads and consistently lower LYE under moderate load ($p < 0.01$).

Functional connectivity analysis (Fig. 5(c)) demonstrates load-dependent reorganization at the network level. Low load is characterized by sparse connectivity and weak long-range interactions, indicating limited cross-regional integration and a predominance of localized processing. Mid load strengthens frontal–parietal and parietal-occipital interactions, resulting in a more integrated and efficient network architecture. This intermediate state likely reflects optimal engagement of executive control, visuospatial processing, and working memory systems, consistent with theories of cognitive resource allocation. In contrast, high load reduces global integration, producing fragmented networks and impaired information transfer, a pattern associated with cognitive overload, diminished attentional control, and reduced neural efficiency in clinical populations.

Complementing these network-level observations, the connectivity matrices (Fig. 5(d)) highlight load-dependent patterns of inter-regional interactions. Under moderate cognitive load, overall connectivity is higher, with strong functional links between occipital and frontal regions, reflecting efficient integration across sensory and executive networks. In contrast, low and high load conditions show limited frontal connectivity, despite some occipital interactions being preserved. Notably, high load is associated with a reduction in long-range connections, reflecting fragmented network organization under excessive cognitive demand. These results corroborate the trajectory- and LYE-based findings, emphasizing that moderate cognitive load promotes stable, integrated, and functionally efficient brain dynamics.

D. Assessment for Real-time Brain Activity

Classification experiments were conducted to evaluate the effectiveness of the proposed spatiotemporal dynamical features in assessing cognitive load. The performance of each model was assessed using 5-fold cross-validation. A variety of classification approaches were compared, including conventional machine learning methods (SVM, LSTM, GCNN), typical EEG deep learning models (EEGNet, DeepConvNet, EEG Transformer), and temporal convolutional networks (TCN). For these comparison models, the preprocessed EEG signals were directly utilized as inputs. All deep learning models were trained for 100 epochs using a batch size of 4, a learning rate of $1e^{-4}$, and the cross-entropy loss function. The proposed DL-based framework was additionally evaluated for comparison. All models are trained across all subjects. Classification results are summarized in Table III, including accuracy, precision, recall, F1-score, and Cohen's kappa.

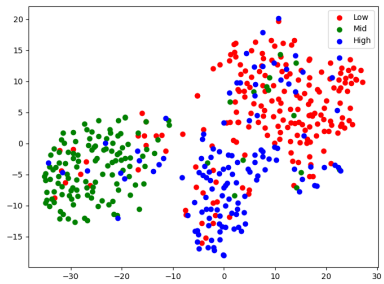

Fig. 6. t-SNE Visualization of Cognitive Load Classes Based on Spatiotemporal Dynamic Feature Extraction Using the Proposed Method.

Among all methods, traditional machine learning models achieved moderate performance, reflecting limited capability to capture complex EEG spatiotemporal dynamics. Representative deep learning models improved performance, with higher accuracy, F1-score, and kappa score, indicating better extraction of neural features. TCN slightly outperformed these baselines. Notably, the proposed DL-based framework achieved the highest performance across all metrics, with 77.08% accuracy, 77.10% precision, 76.51% recall, 76.54% F1-score, and 0.65 kappa. These results confirm that incorporating nonlinear EEG spatiotemporal characteristics enables more accurate and robust cognitive load classification, consistent with observations from reconstructed dynamical trajectories, Lyapunov exponent topographies, functional connectivity, and subjective scale scores.

t-distributed Stochastic Neighbor Embedding (t-SNE) was applied to visualize the feature distributions of the three cognitive load classes, further assessing the discriminative capability of the proposed features. As shown in Fig. 6, samples corresponding to low, mid, and high cognitive load form three well-separated clusters in the embedded space, exhibiting minimal overlap between adjacent classes. This clear separation demonstrates that the proposed model effectively captures discriminative spatiotemporal and nonlinear dynamical patterns. The observed clustering aligns with EEG trajectories, Lyapunov exponent maps, functional connectivity results, and subjective scale scores, further validating the robustness and suitability of the extracted features for adaptive cognitive load assessment.

E. Evaluation of Proposed HRCI Training Paradigm

To validate the effectiveness of the proposed paradigm for dynamically adjusting HRCI parameters based on spatiotemporal brain dynamics, participants completed standardized questionnaires, including STAI-S and VAS-F, before and after each session. These assessments were designed to

TABLE IV

SUBJECTIVE SCALE SCORES

Subject	Gender	Age	STAI-S				VAS-F			
			Non-Adaptive-Pre	Non-Adaptive-Post	Adaptive-Pre	Adaptive-Post	Non-Adaptive-Pre	Non-Adaptive-Post	Adaptive-Pre	Adaptive-Post
S1	Male	23	47	44	47	40	22	20	21	18
S2	Female	21	48	46	48	40	24	23	20	16
S3	Male	25	49	49	51	49	10	10	10	10
S4	Male	25	47	46	46	45	21	22	22	18
S5	Male	20	42	41	40	32	18	19	23	14
S6	Male	23	48	46	48	40	22	20	21	18
Average	-	22.8 ± 2.0	45.8 ± 1.2	44.3 ± 1.4	45.7 ± 1.6	40.3 ± 2.6	21.8 ± 3.5	21.0 ± 2.9	19.0 ± 1.9	14.8 ± 1.3
p-within			**0.02***		**0.01***		0.34		**0.02***	
p-between			**0.02***				**0.04***			

capture changes in cognitive decision-making ability. Table IV presents both within-paradigm pre–post comparisons and between-paradigm differences across the questionnaires, providing quantitative evidence that the proposed approach modulates cognition and affect. The results showed that participants' scores significantly decreased after the paradigm training. A t-test confirmed the presence of statistical differences between pre- and post-training scores. Furthermore, t-test comparing the adaptive paradigm with the non-adaptive protocol demonstrated greater score reductions, with statistically significant differences. Reconstructed topographical maps, functional connectivity networks, and connectivity matrices were visualized in Fig. 7 to objectively assess participants' brain spatiotemporal dynamics under the adaptive paradigm. The results consistently show that, under the adaptive HRCI, participants' brain states were maintained within a moderate cognitive load range. Moreover, the dynamic organization of brain regions was more structured, with a higher number of stable and coherent functional connections. These observations suggest that the proposed paradigm enhances cognitive performance, as reflected in questionnaire scores, and promotes orderly and integrated neural dynamics, supporting efficient information processing and adaptive cognitive regulation during training.

V. DISCUSSION AND CONCLUSION

In this study, we proposed and validated a novel framework for assessing brain activity during a human–robot interaction paradigm. By conceptualizing the brain as a complex nonlinear dynamical system and leveraging deterministic learning principles, the proposed approach surpasses traditional linear or static assessments, capturing both temporal evolution of neural signals and spatial connectivity across cortical regions. The extracted spatiotemporal features provide an interpretable, physiologically grounded view of neural states, enabling more precise identification of cognitive load levels and improved decision-making performance. Key findings demonstrate that applying this framework within the paradigm significantly improves cognitive decision-making, highlighting its potential for real-time adaptive training and personalized human–robot interaction.

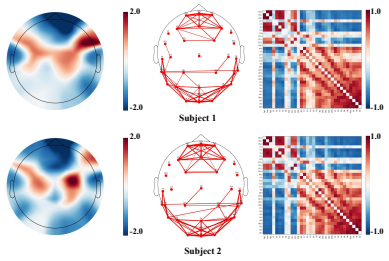

Fig. 7. Spatiotemporal visualization of brain activity for different subjects.

REFERENCES

[1] Y. Liao, M. Cao, X. Xu, *et al.*, "Atom: Adaptive Theory-of-Mind-Based Human Motion Prediction in Long-Term Human-Robot Interactions," in *IEEE International Conference on Robotics and Automation*, 2025.

[2] J. Fan, L. C. Mion, L. Beuscher, *et al.*, "SAR-Connect: A Socially Assistive Robotic System to Support Activity and Social Engagement of Older Adults," in *IEEE Transactions on Robotics*, vol. 38, no. 2, pp. 1250–1269, 2022.

[3] J. Han, Y. Li, X. Gu, *et al.*, "An EEG Conformer Model for Error Feedback During Human-Robot Interaction," in *IEEE International Conference on Robotics and Automation*, 2025.

[4] Y. Xu, A. Uppal, M. S. Lee, *et al.*, "Earable multimodal sensing and stimulation: a prospective towards unobtrusive closed-loop biofeedback," in *IEEE Reviews in Biomedical Engineering*, 2024.

[5] E. Murphy, G. Poudel, S. Ganesan, *et al.*, "Real-time fMRI-based neurofeedback to restore brain function in substance use disorders: a systematic review of the literature," in *Neuroscience & Biobehavioral Reviews*, vol. 165, p. 105865, 2024.

[6] M. Fastenrath, K. J. Friston, S. J. Kiebel, "Dynamical causal modelling for M/EEG: spatial and temporal symmetry constraints," in *Neuroimage*, vol. 44, no. 1, pp. 154–163, 2009.

[7] P. Li, X. Gao, C. Li, *et al.*, "Granger causal inference based on dual Laplacian distribution and its application to MI-BCI classification," in *IEEE Transactions on Neural Networks and Learning Systems*, 2023.

[8] K. Shi, R. Huang, J. Lyu, *et al.*, "EEG-Based Motor Imagery Classification With Tuned Heuristic Fusion Graph Convolutional Network for Rehabilitation Training," in *IEEE Transactions on Automation Science and Engineering*, vol. 22, pp. 14928–14939, 2025.

[9] C. Xu, H. Sang, C. Zhang, *et al.*, "NeuTRL: Neural Trust-Guided Reinforcement Learning for Human-Robot Collaboration," in *IEEE Robotics and Automation Letters*, vol. 10, no. 8, pp. 8155–8162, 2025.

[10] H. Wang, J. Hao, Z. Sun, *et al.*, "Online Hand Movement Recognition System with EEG-EMG Fusion Using One-Dimensional Convolutional Neural Network," in *IEEE/RSJ International Conference on Intelligent Robots and Systems*, 2024.

[11] S. Chen, R. Zheng, T. Wang, *et al.*, "Deterministic learning-based WEST syndrome analysis and seizure detection on ECG," in *IEEE Transactions on Circuits and Systems II: Express Briefs*, vol. 69, no. 11, pp. 4603–4607, 2022.

[12] W. Wu, H. Sun, Z. Teng, *et al.*, "A new method for the assessment of adenoid hypertrophy: Respirdynamicsgram (RDG)," in *Biomedical Signal Processing and Control*, vol. 85, p. 105005, 2023.

[13] M. Deng and C. Wang, "Gait recognition under different clothing conditions via deterministic learning," in *IEEE/CAA Journal of Automatica Sinica*, vol. 11, no. 6, pp. 1530–1532, 2018.

[14] L. Zhang, M. Lei, J. Zhang, *et al.*, "Engaging Mind and Body: An Immersive BCI Paradigm with Motion-Panoramic Virtual Reality," in *IEEE/RSJ International Conference on Intelligent Robots and Systems*, 2025.

[15] J. C. Robinson, "All possible chaotic dynamics can be approximated in three dimensions," in *Nonlinearity*, vol. 11, no. 3, p. 529, 1998.